Journal of Hazardous Materials 188 (2011) 132–139

Contents lists available at ScienceDirect

Journal of Hazardous Materials

journal homepage: www.elsevier.com/locate/jhazmat

Catalytic combustion of chlorobenzene over Mn-Ce-La-O mixed oxide catalysts

Dai Yu, Wang Xingyi*, Li Dao, Dai Qiguang

Laboratory for Advanced Materials, Research Institute of Industrial Catalysis, East China University of Science and Technology, Shanghai 200237, China

ARTICLE INFO

Article history:
Received 24 November 2010
Received in revised form 14 January 2011
Accepted 18 January 2011
Available online 26 January 2011

Keywords:
Chlorobenzene
MnO_x
La_2O_3
CeO_2
Catalytic combustion

ABSTRACT

A series of Mn(x)-CeLa mixed oxide catalysts with different compositions prepared by sol–gel method were tested for the catalytic combustion of chlorobenzene (CB), as a model of chlorinated aromatics. Mn(x)-CeLa catalysts with the ratios of Mn/(Mn + Ce + La) in the range from 0.69 to 0.8 were found to possess high catalytic activity in the catalytic combustion of CB. The stability and deactivation of Mn(x)-CeLa catalysts were studied by other assistant experiments. Mn(x)-CeLa catalysts can deactivate below 330 °C, due to the strong adsorption of Cl species produced during the decomposition of CB. Nevertheless, the increase in oxygen concentration can enhance the resistance to Cl poisoning through the reaction of surface oxygen species with residual chlorine. At 350 °C, high activity, good selectivity and desired stability were observed over Mn(x)-CeLa catalysts.

1. Introduction

Aryl chlorides are hazardous pollutants that are considered among the most harmful organic contaminants due to their acute toxicity and strong bioaccumulation potential [1], and therefore, the safe disposal of aryl chloride pollutants has acquired great importance with the ever increasing concern for environmental protections [2]. Among various available detoxification techniques, catalytic combustion is an interesting one which can be efficiently performed. Of studies of the catalysts used in the catalytic combustion of aryl chlorides, most have reported on the three types of catalysts based on noble metals, transition metals and zeolites [3–5]. At present, the problems such as the formation of polychlorinated compounds during treatment process and deactivation of catalysts due to adsorption of Cl species on the active sites remain yet to be solved. Therefore, the development of catalysts having high performance in converting aryl chlorides is of great significance.

Among the catalysts used for catalytic combustion of aryl chlorides, manganese oxides, either the supported or the unsupported, are the preferred ones [6]. The recently developed Mn based catalysts, i.e., $MnCeO_x$ mixed oxides prepared by the sol–gel method have been reported about the high activity in catalytic combustion of chlorobenzene (CB) [7,8]. Activity and stability of $MnCeO_x$ mixed oxides are found to be related to the particle size of $MnCeO_x$ solid solution which has a fluorite-like structure with a large amount of surface oxygen adequately supplied to the oxidation for the final removal of the formed chloride species. But the thermal stability of structure of $MnCeO_x$ solid solution still involves many problems to be tackled.

As known, La_2O_3, as additive or support, has been widely investigated due to its thermal stability and diverse crystalline phases. La_2O_3 can interact with transitional oxides to form perovskite-structured mixed oxides, ABO_3, of which $LaMnO_3$, modified by doping metal ions, presented high activity and selectivity in the oxidation of methane [9,10]. Moreover, La can promote the thermal stability through the formation of solid solution with other oxides, such as Ce–La–O [11], Al–La–O [12]. In our previous work, it has been found that Mn-based solid solution showed highly activity for the catalytic oxidation of CB, but the transformation of Mn-based solid solution was observed in the thermal treatment. In practice, the thermal stability of the catalysts used for catalytic combustion of CB is of great concern. Here, the incorporation of La into $MnCeO_x$ solid solution may offer an opportunity to prepare novel Mn(x)-CeLa catalysts with high performance for the catalytic oxidation of CB.

2. Experimental

2.1. Catalysts preparation

Mn(x)-CeLa mixed oxides were prepared by sol–gel method: an aqueous solution containing $Mn(NO_3)_2$, $Ce(NO_3)_3{\cdot}6H_2O$ (SCRC, 99.0%), $La(NO_3)_3{\cdot}6H_2O$ (SCRC, 99.0%), and citric acid (SCRC, 99.0%; citric acid/(Mn/1.5 + Ce + La) = 0.3, molar ratio) was gradually

* Corresponding author at: P.O. 396, East China University of Science and Technology, 130 Meilonglu, Shanghai 200237, China. Tel.: +86 21 64253372; fax: +86 21 64253372.
E-mail address: wangxy@ecust.edu.cn (W. Xingyi).

0304-3894/$ – see front matter © 2011 Elsevier B.V. All rights reserved.
doi:10.1016/j.jhazmat.2011.01.084

heated to 80 °C and kept at this temperature for 7 h with stirring, resulting in the formation of an yellowish gel. It was then dried at 110 °C for 12 h and calcined at 650 °C for 5 h in air. The synthesized catalysts are denoted as Mn(x)-CeLa, where x represents the molar ratio for Mn/(Mn + Ce + La). The same method was employed in preparation of CeO_2, Mn(x)-La (x presents the molar ratio for Mn/(Mn + La)) and CeLa catalysts which are used as referenced samples compared with Mn(x)-CeLa.

2.2. Catalysts characterization

The powder X-ray diffraction patterns (XRD) of the samples were recorded on a Rigaku D/Max-rC powder diffractometer using Cu Kα radiation (40 kV and 100 mA). The diffractograms were recorded within the 2θ range of 10–80° with a 2u step size of 0.018 and a step time of 10 s. The nitrogen adsorption and desorption isotherms were measured at −196 °C on an ASAP 2400 system in static measurement mode, and specific surface area was calculated by BET model. The XPS measurements were made on a VG ESCALAB MK II spectrometer by using Mg Kα (1253.6 eV) radiation as the excitation source with the resolution of ±0.2 eV. The Raman spectra were obtained on a Renishaw in Viat + Reflex spectrometer equipped with a CCD detector at ambient temperature and moisture-free conditions. H_2-temperature programming reduction (H_2-TPR) was investigated by heating the samples from 20 to 750 °C in 5 vol.% H_2/Ar flow of 30 ml/min at a heating rate of 10 °C/min. H_2-TPR analyses proceeded with samples were first heated for 60 min in Ar flow at 350 °C, and then treated in O_2 at room temperature for 30 min.

2.3. Catalytic activity measurement

Catalytic combustion reactions were carried out at atmospheric pressure in a continuous flow micro-reactor made of a quartz tube with inner diameter of 4 mm. 200 mg catalyst was packed as the reaction bed. The feeding flow rate to the reactor was set at 50 $cm^3\ min^{-1}$ and the gas hourly space velocity (GHSV) was maintained at 15,000 h^{-1}. Feed stream to the reactor was prepared by delivering liquid CB with a syringe pump into dry air flow, which was metered by a mass flow controller. The injection point is electrically heated to ensure complete evaporation of CB. Moreover, concentration of CB in the feed stream was set at 1000 ppm. The temperature of reaction was measured and controlled with a thermocouple located just at the hot spot of catalyst bed, which is determined by moving the thermocouple up and down within the catalyst bed and the highest temperature was thus recorded. The average deviation of reaction temperature is 0.2–0.5%. The effluent gases were analyzed on-line by using gas chromatographs with FID detector (Fulin 9790 equipped with an AC20 column) within ±1.5% of the average deviation.

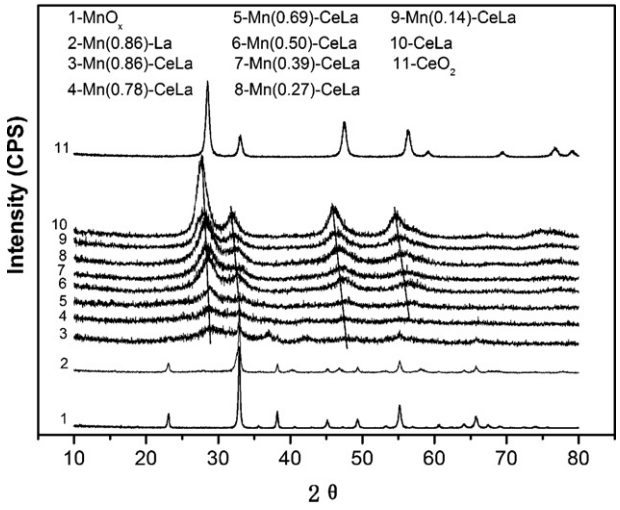

Fig. 1. XRD patterns of Mn(x)-CeLa mixed oxide catalysts with different ratios of Mn/(Mn + Ce + La).

3. Results and discussion

3.1. Catalyst characterization

Wide angle XRD patterns of Mn(x)-CeLa mixed oxide catalysts with different ratios of Mn/(Mn + Ce + La) (at./at.) (for all catalysts, Ce/La = 1) are shown in Fig. 1. The diffractogram of CeO_2 shows the diffraction peaks (at 28.6°, 33.3°, 47.5°, 56.5° and 59.2°) of cerianite characterized with a fluorite-like structure (JCPDS #43-1002). A more asymmetric shape of such reflections with a lower intensity confirms the weakening degree of the crystallinity of samples with the increase in Mn/(Mn + Ce + La) ratio from 0 to 0.86, which is consistent with the increase in surface area (see Table 1). Indeed, the average particle size of ceria, estimated according to the Scherrer equation applied to ⟨1 1 1⟩ crystal plane of cerianite, is inversely related to the surface area (Table 1), which denotes significant contribution of the matrix to surface area exposure.

Moreover, the diffraction peaks of Mn(x)-CeLa mixed oxide catalysts with cubic fluorite-like structure shift gradually to higher values of Bragg angles with the increase in ratio of Mn/(Mn + Ce + La) from 0.5 to 0.86, indicating that part of manganese species can enter the fluorite lattice to form $MnCeO_x$ solid solutions [13]. As reported in Reference [14], the ionic radius of Mn^{3+} (0.066 nm) is smaller than that of Ce^{4+} (0.094 nm), and the incorporation of Mn^{3+} into the fluorite lattice will result in the decrease in lattice parameters. The results shown in Table 1 can justify this phenomenon and confirm the fact that appreciable decrease in ceria particle size parallels with an increase in the Mn amount. As known, the possibility of the incorporation of La^{3+} into fluorite lattice to form $LaCeO_x$ solid solu-

Table 1
The data from XRD patterns of Mn-Ce-La-O catalysts with different compositions.

Catalysts	$d_{111(CeO_2)}$ (Å)	Surface area (m^2/g)	$D_{(CeO_2)}$ (nm)	Lattice parameter$_{(CeO_2)}$ (Å)
MnO*x*		9		
Mn(0.86)-Ce-La	3.09	64.8	5.6	5.36
Mn(0.78)-Ce-La	3.10	70.7	5.9	5.38
Mn(0.69)-Ce-La	3.08	46.4	6.7	5.34
Mn(0.50)-Ce-La	3.12	36.5	7.6	5.40
Mn(0.39)-Ce-La	3.14	30.0	8.57	5.43
Mn(0.27)-Ce-La	3.14	13.1	8.21	5.44
Mn(0.14)-Ce-La	3.16	19.3	8.41	5.48
CeO_2	3.13	5.8	13.9	5.41
Ce-La	3.21	6.0	8.55	5.56
Mn(0.86)-La	–	13.2	–	–

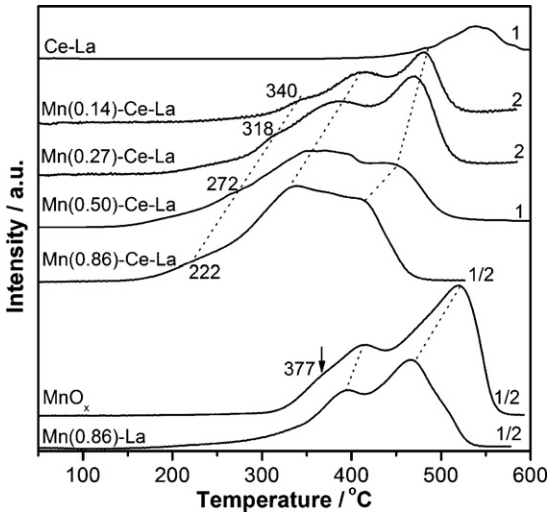

Fig. 2. TPR profiles of Mn(x)-CeLa catalysts with different ratio Mn/(Mn + Ce + La).

tions can exist [11,15]. The ionic radius of La^{3+} (0.106 nm) is larger than that of Ce^{4+}, and the lattice parameter will increase with the incorporation of La^{3+} into the fluorite lattice [16]. Compared with this values in the range of 5.35–5.39 Å obtained from $MnCeO_x$ solid solutions with different ratios of Mn/(Mn + Ce) [17], it can be found that Mn(x)-CeLa catalysts with the ratio of Mn/(Mn + Ce + La) from 0.5 to 0.86 present the similar lattice parameter of fluorite to that of corresponding $MnCeO_x$ catalysts (Table 1). Therefore, $MnCeO_x$ solid solutions dominate for Mn(x)-CeLa catalysts. However, for catalysts with the Mn/(Mn + Ce + La) ratio below 0.5, the diffraction peaks of cubic fluorite-like structure shift gradually to lower values of Bragg angles, and the lattice parameter becomes much larger than 5.41 Å, which is for CeO_2 (Table 1), indicating that La^{3+} gradually incorporate into fluorite to form Ce–La solid solution [18].

In addition to the reflections of the cerianite, no other diffractograms were observed on Mn(x)-CeLa catalysts, except for Mn(0.86)-CeLa catalyst, on which the reflections from α-Mn_2O_3 at 32.9°, 38.13°, 49.56°, 55.17° and 65.77° (JCPDS #24-0508) [19] and MnO_2 at 37.2° and 42.3° [18,19] are observed. The crystalline phase corresponding to La species, such as La_2O_3 (49.27° and 45.18°) and $LaMnO_3$ (40.12°, 46.71° and 58.07° (JCPDS #54-1275)), can not observed, due to a high dispersion of La species either into or between fluorite matrix. For Mn(0.86)-La catalyst, weak reflections from $LaMnO_3$ appear.

Reduction peaks on TPR (Fig. 2) profiles result from the reduction of Mn ions belonging to different structures/phases. For MnO_x, two strong reduction peaks appear at 412 and 520 °C, respectively. Assuming that MnO is the final reduction state [20] from various Mn species in the initial MnO_x, it is reasonable to propose that the peak at low temperature could be assigned to the reduction of MnO_2/Mn_2O_3 to Mn_3O_4, and the peak at high temperature corresponds to the reduction of Mn_3O_4 to MnO [21,22]. In the case of Mn(0.86)-La, the addition of La promotes the reduction of Mn, especially the reduction at high temperature which shifts to 470 °C. Moreover, H_2 consumption at the second reduction step becomes greater, implying that the amount of Mn^{3+} is larger than that of Mn^{4+}. This is consistent with XRD results that MnO_x and Mn(0.86)-La mainly present in α-Mn_2O_3 phase.

The reduction of CeLa catalyst occurs at 544 °C, associated with the reduction of surface Ce^{4+} ions [19], consuming less H_2 as compared with the reduction features of pure MnO_x. With the addition of Ce and La into MnO_x, the reduction temperatures systematically shift to lower values with the increase in the amount of Mn. Mn(0.86)-CeLa is reduced at the lowest temperature. Two broad overlapped reduction peaks assigned to the reduction of MnO_2/Mn_2O_3 and Mn_3O_4 appear around 331 and 415 °C, respectively. On the left side of low temperature, it can be observed that the shoulder peak appears at 223 °C, which can be related to the presence of "isolated" Mn^{4+} ions that "embedded" into the surface defective positions of ceria lattice. Furthermore, H_2 consumption at the first step is larger than that at the second step, indicating that more Mn^{4+} ions can exist. With the decrease in the amount of Mn, the reduction temperatures at different steps become gradually high. As known, the reduction of Mn species is promoted by a high degree of coordinative unsaturation as in the case of $MnCeO_x$, greatly by neighboring Ce^{4+} ions [23]. This increase in temperature implies that the chemical environment around Mn species changes, that is, the interaction between Mn and Ce will be weakened with the increase in the amount of La. For Mn(0.14)-CeLa catalyst, two reduction peaks appear at 400 and 479 °C, respectively, similar with those of Mn(0.86)-La.

The characterization of chemical species located in the near-surface region of the catalysts was carried out by XPS and the data are summarized in Table 2. The O 1s spectra in Fig. 3 exhibit two features. The peak at lower binding energy of 529.4–530.0 eV corresponds to lattice oxygen (O^{2-}), whereas the one corresponds to several O ls states assigned to the surface-adsorbed oxygen such as O_2^{2-} or O^-, hydroxyl OH^- and carbonate CO_3^{2-} species (all fall in the 531–532 eV range) and adsorbed molecular water (above 533.0 eV) [24–29]. For CeO_2, O 1s spectrum assigned to lattice oxygen presents the peak at 528.9 eV [23]. With the incorporation of La, this peak shifts to low binding energy and becomes weak. The intensity of peaks in the range of 531.4–532.0 eV becomes obviously strong with the increase of the amount of La, due to the formation of LaOOH and $La_2O_2CO_3$ through the interaction of H_2O and CO_2 in air with La_2O_3 when treated thermally [15]. Moreover, the binding energy of these oxygen species shifts to low values with the increase

Table 2
XPS data of catalysts with different composition.

Catalysts	Element (at.%)			La/Ce (at.)	Mn (at.%)			Mn^{3+}/Mn	La $3d_{5/2}$ (eV)	Mn 2p (eV)
	Mn	Ce	La		Mn^{3+}	Mn^{4+}	Mn shake up			
Mn(0.86)-La	21.1	–	14.9	–	7.0	8.5	5.6	0.33	834.1 838.3	641.1 642.3 644.0
Mn(0.86)-CeLa	29.9	1.6	4.3	2.8	10.3	11.3	7.8	0.34	834.1 838.2	641.1 642.3 644.1
Mn(0.50)-CeLa	12.5	7.9	14.2	1.8	3.0	5.7	3.9	0.24	834.0 838.2	641.1 642.3 643.7
Mn(0.14)-CeLa	2.9	11.4	17.6	1.5	0.6	1.2	1.1	0.21	836.8 840.4	641.6 643.1 644.7
CeLa	–	10.2	15.9	1.5	–	–	–		835.7	–

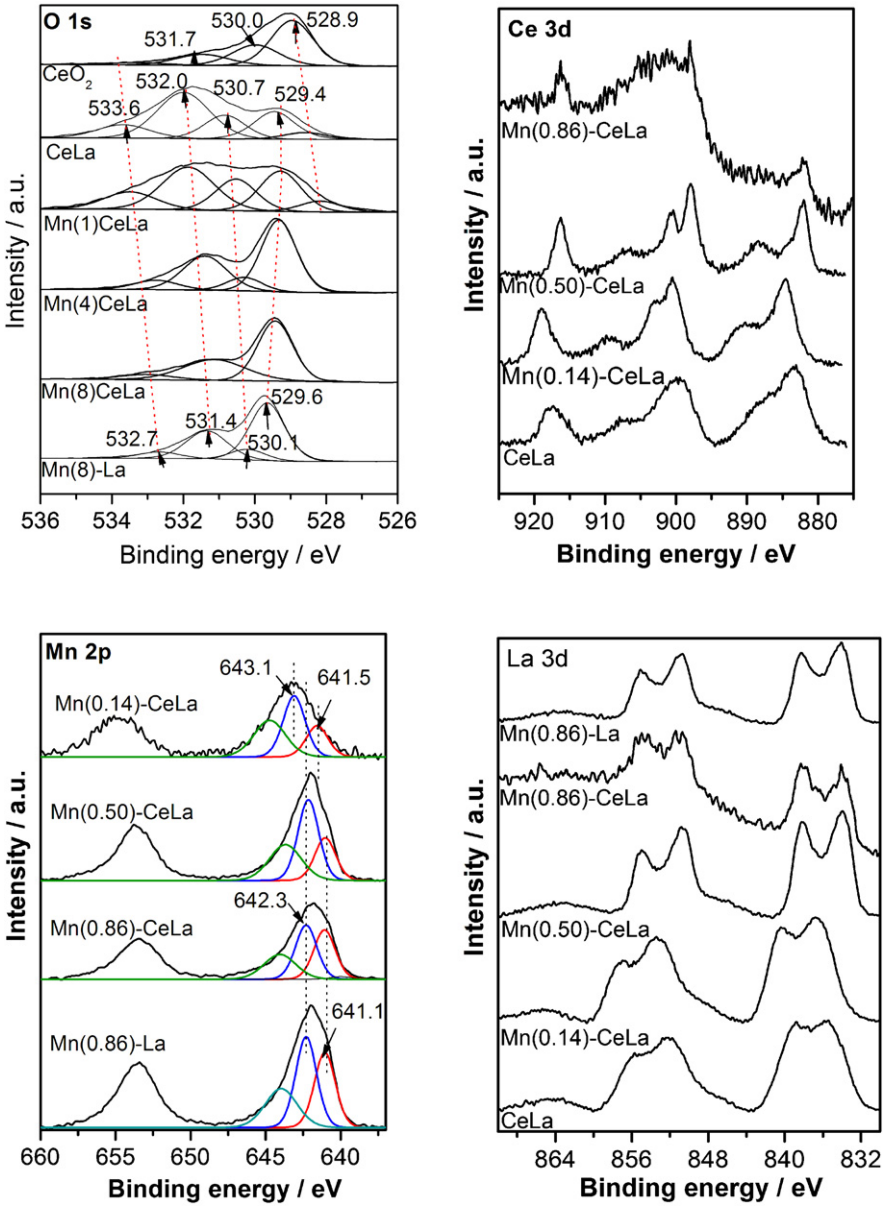

Fig. 3. XPS of elements in the fresh catalysts with different ratio of Mn/(Mn + Ce + La).

in the amount of Mn, and reaches the lowest for Mn(0.86)-La catalyst, indicating that La species disperses into Mn species matrix gradually, and the formation of LaOOH and $La_2O_2CO_3$ is difficult.

The binding energy values of La $3d_{3/2}$ and La $3d_{5/2}$ (the spin–orbit splitting of La was 16.8 eV) are almost constant for Mn(x)-CeLa catalysts and are close to values characteristic of pure lanthanum oxide, i.e., 850 eV for La $3d_{3/2}$ and 834.1–834.0 eV for La $3d_{5/2}$ [26,27]. Small variations were ascribed to the changes in the crystal structure and/or electronic structure. La $3d_{5/2}$ spectrum of the $LaMnO_{3+\delta}$ was deconvoluted to four peaks [30]. The peak at 833.7 eV (in Reference [31] at 833.9 eV) was attributed to La^{3+} of the perovskite and the signal at 835.7 eV to the La^{3+} of lanthanum surface carbonate [30,31]. The peaks at 837.8 and 839.0 eV were interpreted as due to the strong screening effect of f electrons of the two first La^{3+} features [30]. Combining the fact that XRD pattern of Mn(0.86)-La presents $LaMnO_3$ phase, it can be considered that La $3d_{5/2}$ spectra obtained on Mn(0.86)-La, Mn(0.86)-CeLa and Mn(0.50)-CeLa undoubtedly can be assigned to lanthanum ions in trivalent form existing in $LaMnO_3$ phase, while the peaks in La $3d_{5/2}$ spectra for CeLa and Mn(0.14)-CeLa at 835.7–836.4 eV, to the La^{3+} of lanthanum surface carbonate. The Ce 3d core level is shown also in Fig. 3, and the same trend of change as the La 3d level with the decrease in the amount of Mn is observed. The presence of hydroxyl and carbonate on the surface enforces the transfer electron from Ce species to these surface oxygen species.

The binding energies of Mn $2p_{3/2}$ and Mn $2p_{1/2}$ (Table 2) are very similar to those reported in the literature [24,27]. The fitted XPS spectra of Mn 2p are shown in Fig. 3. The component at 641.6–642.9 eV is attributed to Mn^{3+} ions and that at 643.0–644.5 eV to Mn^{4+} ions [27]. No Mn^{2+} is observed on the spectra of catalysts under study. Furthermore, the value of the Mn^{3+}/Mn ratio (Table 2) in the surface layer of Mn(x)-CeLa catalysts is quite low (0.21–0.33), contrasted to those of $MnCeO_x$ catalysts (0.45–0.53) [7], indicating that the incorporation of La affects the electronic valence of Mn species to a significant extent.

According to the element analyses of catalysts shown in Fig. 4, it can be seen that the amount of La on the surface is larger than that in the bulk, while the amount of Ce and Mn, smaller than

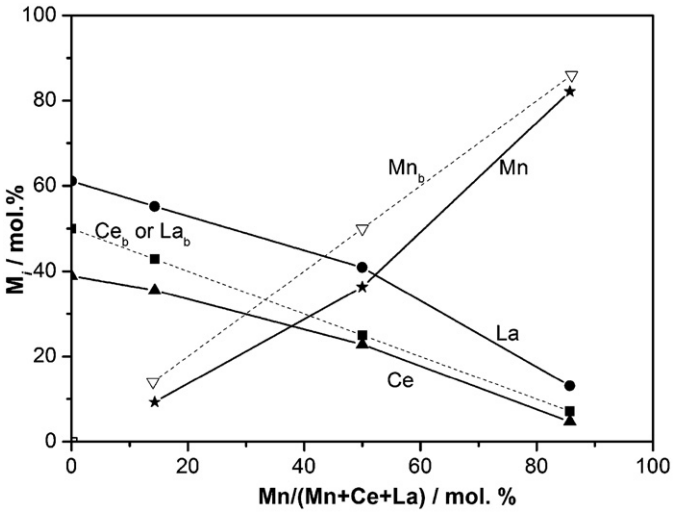

Fig. 4. The contribution of elements on the surface of catalysts estimated by XPS, solid line: Ce (▲), Mn (★) and La (●); dish line: the bulk amounts of Mn (▽) and Ce or La (■).

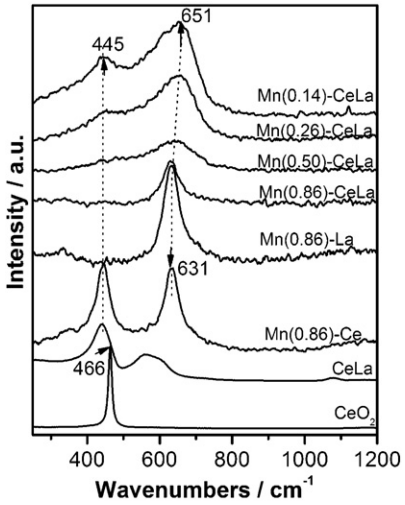

Fig. 5. Raman spectra of the fresh catalysts with different ratio of Mn/(Mn + Ce + La).

that of bulk. Wilkes et al. [15] reported that the enrichment of La occurred on the surface of fluorite-like structure, especially when the amount of La was small related to the amount of Ce. In this work, the ratio of Ce/La for all catalysts containing both Ce and La maintains 1:1. A large number of Mn^{3+} ions enter the fluorite-like structure to form $MnCeO_x$ solid solution, and a certain amount of La^{3+} ions reside in the sites exhibiting high coordinative unsaturation; for example, at low coverage there may be disproportionately high contributions from disordered segregation at steps, edges, and other surface defects [15]. Thus, the incorporation of La should decrease the energy level of fluorite structure when thermally treated. Therefore, the thermal stability of fluorite can be promoted greatly. In this work, this phenomenon was confirmed by the following experimental result: $MnCeO_x$ with the ratio of Mn/(Mn + Ce) of 0.8 prepared by the same method as Mn(x)-CeLa decomposed to lead to the separation of CeO_2 and MnO_x from solid solution after the calcinations at 650 °C.

Raman spectroscopy technique was used for the investigation of the fresh catalysts structure; the spectra obtained are compiled in Fig. 5. The spectra corresponding to catalysts containing La do not present the typical La_2O_3 band at 460 cm^{-1} [32]. The main band of CeO_2 catalyst at 466 cm^{-1} is the only allowed Raman mode (F2g) of fluorite-type structure [33–35]. Fluorite-structure is a cubic structure in which the cations are placed at the corners and in the centers of faces and oxygen atoms are located at the tetrahedral sites. Raman spectra for these fluorite-type oxide structures are dominated by oxygen lattice vibrations and are sensitive to crystalline symmetry [35]. The presence of La^{3+} in the CeO_2 lattice deforms the structure, and the fluorite-characteristic peak intensity decreases significantly. For the same reason, the similar change in the band of CeO_2 occurs with the addition of Mn. Moreover, the addition of either La or Mn causes ν_{F2g} to shift from 466 to 445 cm^{-1}, probably due to a decrease in CeO_2 grain size [36,37], which is opposite to the trendency observed for pure CeO_2, possibly due to the thermal-induced loss of lattice O, which results in the sintering of CeO_2 crystals. The band at 574 cm^{-1} for CeLa catalyst is assigned to the oxygen vacancies in the CeO_2 lattice [38]. For Mn(x)-CeLa catalysts, the deformation of structure of fluorite is enhanced greatly so that the band of CeO_2 gradually become weak quickly with the increase in the amount of Mn and finally disappears from the spectrum for Mn(0.86)-CeLa catalyst. As motioned that the band of CeO_2 is dominated by oxygen lattice vibrations, this phenomenon implies that Ce–O in MnCeLa is highly asymmetric, so that the band of CeO_2 resulted from the oxygen lattice vibrations is divergent. This asymmetric structure can be formed through the binding of Ce–O with both Mn and La species, Mn–O–Ce–O–La. It has been reported that this deformation favors oxygen mobility, affecting the redox behavior of the material [39], which is consistent with our TPR results. With the decrease in the amount of Mn, La will substitute for Mn, and the number of "La–O–Ce–O–La" sites increases, the band 445 at cm^{-1} becomes strong.

In addition to ν_{F2g} at 445 cm^{-1}, a new band appears at 631–651 cm^{-1} (Fig. 5) for Mn(x)-CeLa catalysts. The new band, which is close to that at 655 cm^{-1} observed for the bulk Mn_3O_4 [40,41], can be assigned to a Mn–O–Mn stretching mode of Mn_3O_4-like species ($\nu_{Mn-O-Mn}$), and shifts to high wavenumbers from 631 to 651 cm^{-1} with the increase in the amount of Ce and La. Meanwhile, its intensity becomes strong with the peak broadening, indicating the change in structure of Mn species. Combining with XRD results, it can be considered that the symmetry band of $\nu_{Mn-O-Mn}$ for catalysts with high amount of Mn can be assigned to the presence of Mn_2O_3 or MnO_2, and the broad band of $\nu_{Mn-O-Mn}$, to Mn–O–Mn near Ce or La species on the interface. It is interesting to find that the band of $\nu_{Mn-O-Mn}$ becomes strong with the decrease in the amount of Mn. This implies that Mn species dissociate from the fluorite-structure solid solution.

3.2. The activity of catalysts

The activity tests in Fig. 6A show that Mn(x)-CeLa catalysts appear to be superior for CB catalytic combustion, of which the catalysts with Mn/(Mn + Ce + La) ratio in the range from 0.60 to 0.86 have the best activity, and 90% conversion of CB over the catalysts reaches at GHSV 15,000 h^{-1} at about 229 °C, the temperature being much lower than all those catalysts reported in previous literatures, including noble metal-based catalysts [42,43] or MnO_x/TiO_2-Al_2O_3, MnO_x-CeO_2 and $MnCeO_x/\gamma$-Al_2O_3 catalysts [44–46]. With the decrease of Mn/(Mn + Ce + La) ratio, the activity of catalysts reduces. Fig. 6B shows $T_{50\%}$ and $T_{90\%}$ (the temperature needed for the conversion of 50% and 90%, respectively) as the function of Mn amount; the activity of catalysts increases as the Mn amount increases, except the case of MnO_x. It is interesting to find that $T_{90\%}$ is consistent with the temperature at which Mn^{4+} ions can be reduced, indicating that the reducibility of catalysts is responsible for the activity.

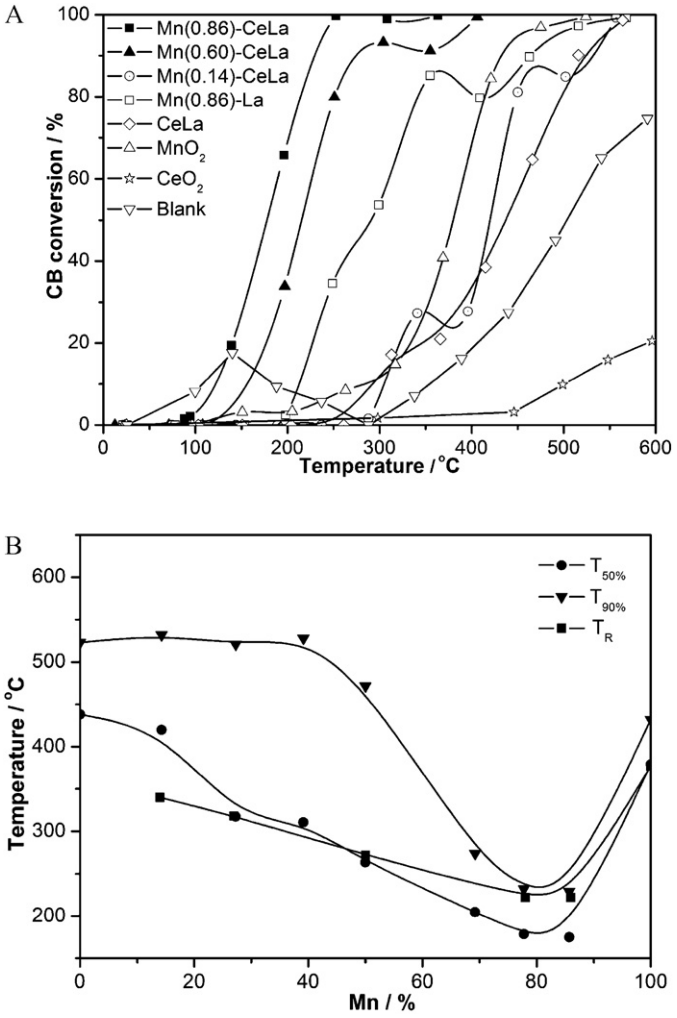

Fig. 6. The activity of the fresh catalysts with different ratios of Mn/(Mn + Ce + La) for CB catalytic combustion (A) conversion of CB; (B) $T_{50\%}$ and $T_{90\%}$; T_R, the reduction temperature of Mn species on the first step; gas composition: 1000 ppm CB, 10% O_2, N_2 balance; GHSV = 15,000 h^{-1}.

Over pure MnO_x, the conversion of CB reaches 90% at 440 °C, higher than that over the Mn(x)-CeLa catalysts with Mn amount in the range 0.6–0.85. CeO_2 presents a higher activity at the initial stage than MnO_x does. However, it begins to deactivate soon as the conversion of CB drops from 18% at 145 °C to 1% at 283 °C. Nevertheless, with the further increase in temperature, the conversion of CB on CeO_2 increases gradually, and reaches 74% at 600 °C. The incorporation of La_2O_3 into CeO_2 improves the activity at high temperature to some extent. Further incorporation of Mn into CeLa improves significantly the activity of catalysts, depending on Mn/(Mn + Ce + La) ratio. For Mn(0.14)-CeLa, $T_{50\%}$ reduces to 419 °C from 507 °C for CeO_2 and its deactivation occurs at higher temperature. With the increase in Mn amount, Mn(x)-CeLa catalysts become more stable in activity, and the deactivation occurs at high conversion.

3.3. The analysis of products

Within the application limits of FID, all the catalysts studied in this experiment provide more than 99.5% selectivity to carbon oxides (more than 98% CO_2 and trace CO) and no polychlorinated benzene or other detectable C-containing by-products are found. This is very different from the case for noble metal-based catalysts

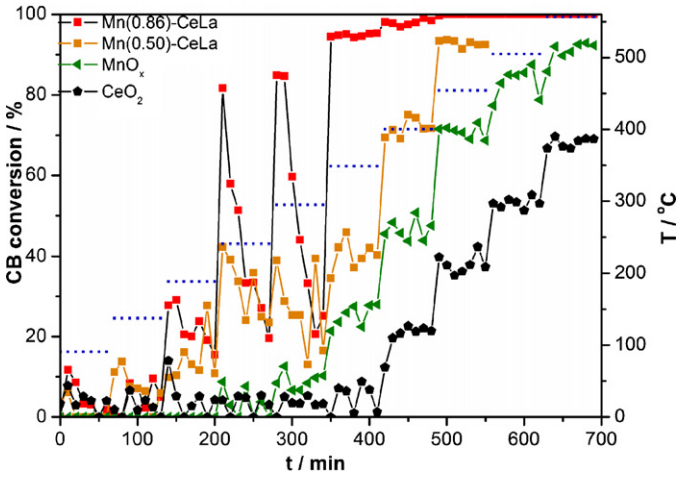

Fig. 7. The stability of catalysts with different ratios of Mn/(Mn + Ce + La) for CB oxidation at different temperature, gas composition: 1000 ppm CB, 10% O_2, N_2 balance; GHSV = 15,000 h^{-1}.

[8,47], over which substantial amount of polychlorinated benzene is formed during the catalytic combustion of CB. Cl balance gives 15–20% less amount in the outlet stream than in the inlet stream; this fact means that deposition of Cl species occurs on the surface of catalysts.

3.4. The stability of catalysts

For the catalytic combustion of CVOCs, the catalyst deactivation is still a hurdle in commercial applications. In previous work, CeO_2 was found rapidly deactivated due to strong adsorption of Cl on active sites during the catalytic combustion of trichloroethylene [48]. In this work, the stability of Mn(x)-CeLa was investigated for the catalytic combustion of CB. Results from the tests conducted at the stepwise-varied temperatures from 50 to 550 °C are presented in Fig. 7, and the variation in activities was observed in 60 min at a given temperature. Conversion of CB vs. the reaction temperature and time was plotted.

As shown, CeO_2 presents an unstable activity and the activity drops quickly as the reaction temperature rises in the range of 100–200 °C, but this drop becomes less obvious in the range of 250–350 °C, probably due to fairly low activity. At higher than 400 °C, CeO_2 achieves a low stable activity without a substantial decrease in conversion. On the contrary, there is not a significant drop in the activity observed on MnO_x, although MnO_x shows fairly low activity. The activity of Mn(x)-CeLa catalysts is improved really at various temperatures with the increase in the amount of Mn. However, their deactivation within 150–300 °C is obvious, and stable activity is reached up to 350 °C, where the conversion of CB on Mn(0.86)-CeLa is 95%. Considering that the reduction of Mn species of Mn(0.86)-CeLa appears at low temperature, its high stable activity can be related to the reducibility of Mn, that is, the removal of Cl species produced during the reaction depends on the supplement of lattice oxygen available for the interaction with Cl species.

The increase in the amount of Cl species during the decomposition of CB should accelerate the deactivation of Mn(0.86)-CeLa catalyst. The change in activity was investigated by increase in the concentration of CB ([CB]) from 1000 ppm to 2500 ppm (Fig. 8) while the oxygen concentration maintains 10%. It can be found that the conversion of CB can be promoted with the increase in temperature in the range of starting value to 240 °C. However, the curves of conversion shifts systematically to high temperature with the increase in [CB] to some extent, indicating that the dependence of [CB] is less than one order, although the reaction rates become

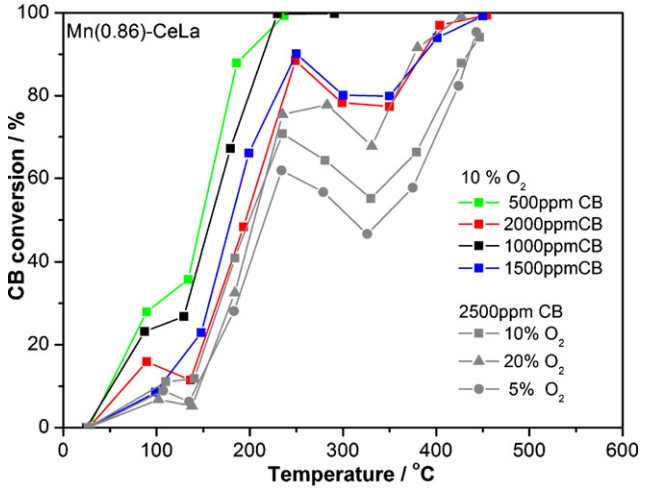

Fig. 8. The effect of CB concentration or oxygen concentration on the activity of the fresh catalysts with different ratios of Mn/(Mn + Ce + La) for CB catalytic combustion; N_2 balance; GHSV = 15,000 h^{-1}.

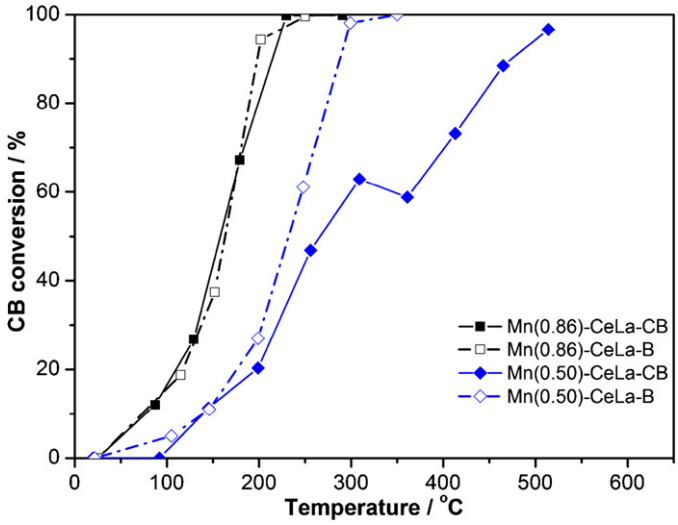

Fig. 9. The comparison of the activity for CB combustion with that for benzene combustion of catalysts with different ratios of Mn/(Mn + Ce + La); -CB and -B, for CB and benzene combustion, respectively; N_2 balance; GHSV = 15,000 h^{-1}; gas composition: 1000 ppm CB or benzene, 10% O_2, N_2 balance; GHSV = 15,000 h^{-1}

great with [CB] at a given temperature. Moreover, the monotonous increase in CB conversion with the increase in the temperature can not observed at 240–323 °C, where, in fact, the reduction of conversion with further increase in the temperature occurs, depending on [CB]. The higher [CB], the larger the conversion reduces. This phenomenon implies that the deactivation of catalyst become more serious when more Cl species are produced. However, the increases in conversion were observed at 323 °C or higher, which is consistent with the temperature on the first step of reduction for Mn(0.86)-CeLa catalyst. The removal of chlorine species can be related to oxygen mobility.

Oxygen concentration [O] is changed from 5% to 20% with maintaining CB concentration to be 2500 ppm, in order to investigate the effect of [O] on the activity (Fig. 8). The trendency of conversion as a function of temperature at different [O] is similar, but the conversion increases significantly with [O], especially 20% O_2. The increase of [O] can promote the removal of Cl species from the surface. Here, there are two possibilities for the promotion of gas oxygen: oxygen mobility which is strongly dependent on [O] is responsible for the removal of Cl species and this surface oxygen species supplement is possible from the gas phase; and oxygen in the gas phase reacts with Cl species. The results obtained from the catalysts with different Mn/(Mn + Ce + La) ratios show the same trendency of increase in the conversion with [O] in gas phase. However, for Mn(0.27)-CeLa catalyst with poor oxygen mobility, the effect of [O] on the CB conversion can hardly be observed, although the significant deactivation of Mn(0.27)-CeLa catalyst was observed. Therefore, the removal of Cl species should be related to the reaction with oxygen species from the surface of catalysts.

The mechanism of catalytic combustion is complex, and involves the activation of reactants and desorption of products. In this work, the combustion of benzene over Mn(0.86)-CeLa and Mn(0.50)-CeLa was investigated. The difference of combustion activity between CB and benzene was observed at high conversion, and increases with the decrease in the Mn amount (Fig. 9). Further test on Mn(0.86)-CeLa catalysts after the treatment in reaction feed containing CB or benzene at 250 °C was carried out (Fig. 10). It is interesting to find that the conversion curves of CB and benzene on the fresh and used catalyst are similar. Considering the difference of reactivity between CB and benzene, including the binding energy of C–H and C–Cl, and the electron drawing of Cl atom, the process involving active oxygen, such as the dissociation of oxygen and the reaction of active oxygen with intermediates of reactants, should be the controlling step, that is, the amount of active oxygen is critical to the oxidation of CB and benzene. The strong adsorption of Cl species on active sites causes the transfer of electron to Cl species and thus the dissociation of gas oxygen species becomes difficult. For a series of Mn(x)-CeLa mixed oxide catalysts, Mn(0.86)-CeLa presents the best reducibility, and thus possesses the best stable activity.

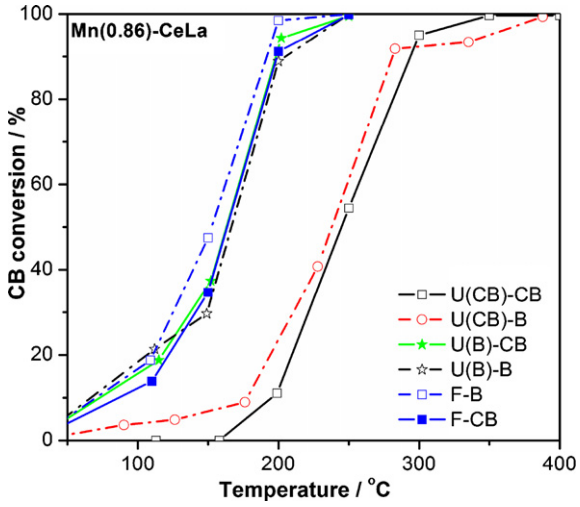

Fig. 10. The activity of Mn(0.86)-CeLa; F, the fresh catalyst; U (B) and U (CB), the used catalysts after CB and benzene combustion at 250 °C for 1 h, respectively; -CB and -B, for CB and benzene combustion, respectively; gas composition: 1000 ppm CB, 10% O_2, N_2 balance; GHSV = 15,000 h^{-1}.

4. Conclusion

In summary, it has been found that Mn(x)-CeLa catalysts present high activity for the low-temperature catalytic destruction of CB. The main products from CB catalytic destruction over the Mn(x)-CeLa catalysts are HCl, Cl_2, CO_2 and trace CO, and polychlorinated compounds has not been detected. Mn(x)-CeLa catalysts with high ratios of Mn/(Mn + Ce + La) present a high stable activity, which is related to their high reducibility and mobility of oxygen for removal of the adsorbed Cl species.

Acknowledgement

We would like to acknowledge the financial support from National Basic Research Program of China (no. 2010CB732300) and National Natural Science Foundation of China (no. 20977029).

References

[1] M.J. Morra, V. Borek, J. Koolpe, Transformation of chlorinated hydrocarbons using aquocobalamin or coenzyme F-430 in combination with zero-valent iron, J. Environ. Qual. 29 (2000) 706–715.
[2] F. Alonso, I.P. Beletskaya, M. Yus, Metal-mediated reductive hydrodehalogenation of organic halides, Chem. Rev. 102 (2002) 4009–4091.
[3] M. Taralunga, B. Innocent, J. Mijoin, P. Magnoux, Catalytic combustion of benzofuran and of a benzofuran/1,2-dichlorobenzene binary mixture over zeolite catalysts, Appl. Catal. B 75 (2007) 139–146.
[4] F.F. Bertinchamps, C. Gregoire, E.M. Gaigneaux, Systematic investigation of supported transition metal oxide based formulations for the catalytic oxidative elimination of (chloro)-aromatics: Part I: identification of the optimal main active phases and supports, Appl. Catal. B 66 (2006) 1–9.
[5] M. Taralunga, J. Mijoin, P. Magnoux, Catalytic destruction of 1,2-dichlorobenzene over zeolites, Catal. Commun. 7 (2006) 115–121.
[6] C.N. Costa, V.N. Stathopoulos, V.C. Belessi, A.M. Efstathiou, An Investigation of the $NO/H_2/O_2$ (lean-deNO_x) reaction on a highly active and selective $Pt/La_{0.5}Ce_{0.5}MnO_3$ catalyst, J. Catal. 197 (2001) 350–364.
[7] X.Y. Wang, Q. Kang, D. Li, Catalytic combustion of chlorobenzene over MnOx–CeO_2 mixed oxide catalysts, Appl. Catal. B 86 (2009) 166–175.
[8] X.Y. Wang, Q. Kang, D. Li, Low-temperature catalytic combustion of chlorobenzene over MnO_x–CeO_2 mixed oxide catalysts, Catal. Commun. 9 (2008) 2158–2162.
[9] M. van den Bossche, S. McIntosh, The rate and selectivity of methane oxidation over $La_{0.75}Sr_{0.25}Cr_xMn_{1-x}O_{3-\delta}$ as a function of lattice oxygen stoichiometry under solid oxide fuel cell anode conditions, J. Catal. 255 (2008) 313–323.
[10] A. Machocki, T. Ioannides, B. Stasinska, W. Gac, G. Avgouropoulos, D. Delimaris, W. Grzegorczyk, S. Pasieczna, Manganese–lanthanum oxides modified with silver for the catalytic combustion of methane, J. Catal. 227 (2004) 282–296.
[11] B. Zhang, D. Li, X.Y. Wang, Catalytic performance of La–Ce–O mixed oxide for combustion of methane, Catal. Today 158 (2010) 348–353.
[12] X.Y. Chen, Y. Liu, G. Niu, Z.X. Yang, M.Y. Bian, A.D. He, High temperature thermal stabilization of alumina modified by lanthanum species, Appl. Catal. A 205 (2001) 159–172.
[13] M. Machida, M. Uto, D. Kurogi, T. Kijima, MnO_x–CeO_2 binary oxides for catalytic NO_x sorption at low temperatures. Sorptive removal of NO_x, Chem. Mater. 12 (2000) 3158–3164.
[14] D. Terribile, A. Trovarelli, C. De Leitenburg, A. Primavera, G. Dolcetti, Catalytic combustion of hydrocarbons with Mn and Cu-doped ceria–zirconia solid solutions, Catal. Today 47 (1999) 133–140.
[15] M.F. Wilkes, P. Hayden, A.K. Bhattacharya, Catalytic studies on ceria lanthana solid solutions III. Surface segregation and solid state studies, J. Catal. 219 (2003) 305–309.
[16] M.F. Wilkes, P. Hayden, A.K. Bhattacharya, Surface segregation of lanthanum and cerium ions in ceria/lanthana solid solutions: comparison between experimental results and a statistical–mechanical model, Appl. Surf. Sci. 206 (2003) 12–19.
[17] L. Dimesso, L. Heider, H. Hahn, Synthesis of nanocrystalline Mn-oxides by gas condensation, Solid State Ionics 123 (1999) 39–46.
[18] F. Arena, E. Alongi, P. Famulari, A. Parmaliana, G. Trunfio, Basic evaluation of the catalytic pattern of the $CuCeO_x$ system in the wet oxidation of phenol with oxygen, Catal. Lett. 107 (2006) 39–46.
[19] F. Arena, G. Trunfio, J. Negro, B. Fazio, L. Spadaro, Basic evidence of the molecular dispersion of $MnCeO_x$ catalysts synthesized via a novel "redox-precipitation" route, Chem. Mater. 19 (2007) 2269–2276.
[20] F. Kapteijn, L. Singoredjo, A. Andreini, Activity and selectivity of pure manganese oxides in the selective catalytic reduction of nitric oxide with ammonia, Appl. Catal. B 3 (1994) 173–189.
[21] J. Carnö, M. Ferrandon, E. Björnbom, S. Järås, Mixed manganese oxide/platinum catalysts for total oxidation of model gas from wood boilers, Appl. Catal. A 155 (1997) 265–281.
[22] J. Trawczyński, B. Bielak, W. Miśta, Oxidation of ethanol over supported manganese catalysts—effect of the carrier, Appl. Catal. B 55 (2005) 277–285.
[23] S.T. Hussain, A. Sayari, F. Larachi, Enhancing the stability of Mn–Ce–O WETOX catalysts using potassium, Appl. Catal. B 34 (2001) 1–9.
[24] S. Ponce, M.A. Pena, J.L.G. Fierro, Surface properties and catalytic performance in methane combustion of Sr-substituted lanthanum manganites, Appl. Catal. B 24 (2000) 193–205.
[25] Y. Ng Lee, R.M. Lago, J.L. Fierro, V. Cortes, F. Sapina, E. Marinez, Surface properties and catalytic performance for ethane combustion of $La_{1-x}K_xMnO_{3+\delta}$ perovskites, Appl. Catal. A 207 (2001) 17–24.
[26] M. O'Connell, A.K. Norman, C.F. Hüttermann, M.A. Morris, Catalytic oxidation over lanthanum-transition metal perovskite materials, Catal. Today 47 (1999) 123–132.
[27] Y. Zhang, J. Beckers, A. Bliek, Surface properties and catalytic performance in CO oxidation of cerium substituted lanthanum–manganese oxides, Appl. Catal. A 235 (2002) 79–92.
[28] Y. Ng Lee, R.M. Lago, J.L.G. Fierro, J. González, Hydrogen peroxide decomposition over $Ln_{1-x}A_xMnO_3$ (Ln = La or Nd and A = K or Sr) perovskites, Appl. Catal. A 215 (2001) 245–256.
[29] Z. Yu, L. Gao, S. Yuan, Y. Wu, Solid defect structure and catalytic activity of perovskite-type catalysts $La_{1-x}Sr_xNiO_{3-\lambda}$ and $La_{1-1.333x}Th_xNiO_{3-\lambda}$, J. Chem. Soc. Faraday Trans. 88 (1992) 3245–3249.
[30] G. Sinquin, J.P. Hindermann, C. Petit, A. Kiennemann, Perovskites as polyvalent catalysts for total destruction of C_1, C_2 and aromatic chlorinated volatile organic compounds, Catal. Today 54 (1999) 107–118.
[31] G. Sinquin, C. Petit, J.P. Hindermann, A. Kiennemann, Study of the formation of $LaMO_3$ (M = Co, Mn) perovskites by propionates precursors: application to the catalytic destruction of chlorinated VOCs, Catal. Today 70 (2001) 183–196.
[32] A. Bueno-López, K. Krishna, M. Makkee, J.A. Moulijn, Enhanced soot oxidation by lattice oxygen via La^{3+}-doped CeO_2, J. Catal. 230 (2005) 237–248.
[33] A. Nineshige, T. Taji, Y. Muroi, M. Kobune, S. Fujii, N. Nishi, M. Inaba, Z. Ogumi, Oxygen chemical potential variation in ceria-based solid oxide fuel cells determined by Raman spectroscopy, Solid State Ionics 135 (2000) 481–485.
[34] L.N. Ikryannikova, A.A. Aksenov, G.L. Markayan, G.P. Muravieva, B.G. Kostyuk, A.N. Kharlanov, E.V. Linina, The redox treatments influence on the structure and properties of M_2O_3–CeO_2–ZrO_2 (M = Y, La) solid solutions, Appl. Catal. A 210 (2001) 225–235.
[35] M. Fernandez-García, A. Martínez-Arias, A. Iglesias-Juez, C. Belver, A.B. Hungría, J.C. Conesa, J. Soria, Structural characteristics and redox behavior of CeO_2–ZrO_2/Al_2O_3 supports, J. Catal. 194 (2000) 385–392.
[36] G.W. Graham, W.H. Weber, C.R. Peters, R. Usmen, Empirical method for determining CeO_2-particle size in catalysts by Raman spectroscopy, J. Catal. 130 (1991) 310–313.
[37] W.H. Weber, K.C. Hass, J.R. McBride, Raman study of CeO_2: second-order scattering, lattice dynamics, and particle-size effects, Phys. Rev. B 48 (1993) 178–185.
[38] J.R. McBride, K.C. Hass, B.D. Poindexter, W.H. Weber, Raman and X-ray studies of $Ce_{1-x}RE_xO_{2-y}$, where RE = La, Pr, Nd, Eu,Gd, and Tb, J. Appl. Phys. 76 (1994) 2435–2441.
[39] P. Fornasiero, J. Kašpar, M. Grazini, Redox behavior of high surface area Rh-loaded $Ce_{0.5}Zr_{0.5}O_2$ mixed oxide, J. Catal. 167 (1997) 576–580.
[40] Y.F. Han, L.W. Chen, K. Ramesh, E. Widjaja, S. Chilukoti, I.K. Surjami, J.S. Chen, Kinetic spectroscopic study of methane combustion over α-Mn_2O_3 nanocrystal catalysts, J. Catal. 253 (2008) 261–268.
[41] R.J. Charlson, A Stone Age greenhouse, Nature 438 (2005) 165–166.
[42] A. Musialik-Piotrowska, B. Mendyka, Catalytic oxidation of chlorinated hydrocarbons in two-component mixtures with selected VOCs, Catal. Today 90 (2004) 139–144.
[43] R.W. van den Brink, P. Mulder, R. Louw, Catalytic combustion of chlorobenzene on Pt/γ-Al_2O_3 in the presence of aliphatic hydrocarbons, Catal. Today 54 (1999) 101–106.
[44] M. Taralunga, J. Mijoin, P. Magnoux, Catalytic destruction of chlorinated POPs-catalytic oxidation of chlorobenzene over PtHFAU catalysts, Appl. Catal. B 60 (2005) 163–171.
[45] Y. Liu, Z. Wei, Z. Feng, M. Luo, P. Yang, C. Li, Oxidative destruction of chlorobenzene and *o*-dichlorobenzene on a highly active catalyst: MnO_x/TiO_2-Al_2O_3, J. Catal. 202 (2001) 200–204.
[46] M. Wu, X.Y. Wang, Q.G. Dai, Y.X. Gu, D. Li, Low temperature catalytic combustion of chlorobenzene over Mn-Ce-O/γ-Al_2O_3 catalyst, Catal. Today 158 (2010) 336–342.
[47] S.M. de Lima, I.O. da Cruz, G. Jacobs, B.H. Davis, L.V. Mattos, F.B. Noronha, Steam reforming, partial oxidation, and oxidative steam reforming of ethanol over $Pt/CeZrO_2$ catalyst, J. Catal. 257 (2008) 356–368.
[48] Q.G. Dai, X.Y. Wang, G.Z. Lu, Low-temperature catalytic combustion of trichloroethylene over cerium oxide and catalyst deactivation, Appl. Catal. B 81 (2008) 192–202.